RESEARCH ARTICLE

Scavenging malachite green dye from aqueous solution using durian peel based activated carbon

Mohamad Firdaus Mohamad Yusop[a], Mohd Azmier Ahmad[a,*], Nur Ayshah Rosli[a], Fadzil Noor Gonawan[a], Soran Jalal Abdullah[b]

[a] School of Chemical Engineering, Engineering Campus, Universiti Sains Malaysia, 14300 Nibong Tebal, Penang, Malaysia
[b] Department of Technology, Faculty of Innovative Design and Technology, Universiti Sultan Zainal Abidin, Gong Badak Campus, 21300 Kuala Nerus, Terengganu, Malaysia
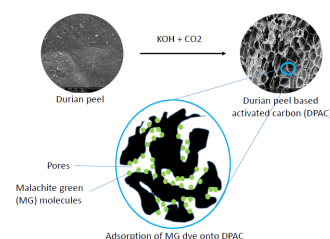
* Corresponding author: chazmier@usm.my

Graphical abstract

Abstract

Physiochemical activation consists of heat treatment coupling with CO_2 gasification and KOH chemical treatment were applied in preparing durian peel based activated carbon (DPAC) to remove basic dye, malachite green (MG) from aqueous solution. Several parameters namely, effect of initial MG concentration as well as contact time, solution temperature and initial solution pH were carried out in this study. Characterization study revealed that DPAC pose high BET surface area which is 886.31 m^2/g and its surface was found to be mesoporous in nature with heterogeneous type of pore structures. Eight isotherms and four kinetic models were utilized and it was revealed that the adsorpttion system followed Freundlich isotherm and pseudo-first order (PFO) kinetic model. Mechanism study using intraparticle diffusion and Boyd plot confirmed that adsorption of MG onto DPAC was controlled by the film-diffusion mechanism. Thermodynamic study indicated that the adsorption system was exothermic, spontaneous, feasible and governed by physical-type of adsorption.
.
Keywords: Adsorption, Activated Carbon, Malachite Green, Physicochemical Activation

INTRODUCTION

Growing demand of clothes from increasing population around the globe had accelerates the development in textile industries. This development is directly proportional to the dyes production. Dyes are essential in giving a final beautification touch to the products (Aderemi et al., 2018). It is estimated that 100,000 dissimilar kind of dyes are commercially exist with yearly production of 0.7 million tons (Vega-Negron et al., 2018). Textile industries encompass an integrated activity ranging from pre-treatment, polymerization, spinning, texturizing, dyeing, printing and made up textile goods. In dyeing operation, most of the wastewater comes from wash water, followed by spent dye bath. Due to dyes' solubility in water, they are easily lost in the effluent during the dyeing processing step (Ahmad et al., 2015). This has been a major concern as it can promote eutrophication and reduce the aesthetic value of the water bodies. Furthermore, the existence of dyes in environment may hurt the textile industries due to their failure to comply with ISO 14000 certification of quality standard specifications (Ayanda et al., 2018).

One of the most popular dye utilized in textile industries is malachite green (MG), a dye that belongs to basic dye group and known as cationic dye. It produces colored cation in solution due to the present of positively charged nitrogen or sulfur atom. MG is applied to paper, polyacrylonitrile, modified nylons, polyesters, silk, wool and tannin-mordanted cotton by forming salt linkages (ionic bonds) with anionic groups in the fiber. Despite of its versatility, numerous concerns had arisen regarding the expanding use of MG due to its toxicity effects such as cytotoxic, genotoxic and mutagenic (Bhatti et al., 2017). Not only in their original form, but the it breakdown products also can be toxic and carcinogenic to the aquatic life (Zhou et al., 2019). Hence, it is essential to treat MG wastewater before entering the environment.

Dyes removal techniques can be categorized into biological, chemical and physical treatments. Biological treatment can be further subcategorized into two types; (i) aerobic process which require oxygen for bacteria to perform degradation process (Khouni et al., 2020, Zhu et al., 2020) and (ii) anaerobic process which operates in the absence of air (Bai et al., 2020, Berkessa et al., 2020). Although biological treatment has advantages such as low cost and absence of chemical waste production, the dyes are not biologically degradable since microorganisms do not utilize the dyes as a source of food. Chemical treatment includes the use of coagulation and flocculation agent in removing dyes from wastewater. However, this method is ineffective to treat dyes that have high solubility in water. Other examples of chemical treatments are oxidation process (Mota et al., 2020), photochemical (Bahadori et al., 2020) and electrochemical degradation (Pereira et al., 2020). The major drawback in chemical treatment is that its application can cause concentrated sludge to accumulate, thus required a further treatment or disposal method.

Physical treatments on the other hand, comprises of adsorption process. Posing several advantages such as simplicity in design, fast, easy to operate, relatively low operating cost and stable towards toxic substance had cause adsorption process to be a popular choice in treating dye wastewater (Machrouhi et al., 2017). Plus, only half or quarter space is required in adsorption process compared to biological

system. Among of the adsorbents, activated carbon is proved to be the most effective one as it has very porous structure resulting large surface area in range 500–2000 m^2/g. This large surface area provides plenty of active sites for the adsorption process to take place. Commercially available activated carbon is produced from non-renewable precursor such as lignite and bituminous coal. These precursors are relatively expensive, thus increasing the total production cost of activated carbon.

There is a growing interest for researchers to convert renewable sources of agricultural wastes into adsorbent. Usually, these wastes are creating disposal problem due to their limitation in application (Aziz et al., 2018). Examples of agricultural wastes include rice straw (Zhu et al., 2018), kernel shell (Zhi and Zaini, 2019), coconut pith (Rahim et al., 2019), coconut flesh waste (Noor et al., 2019), maize corncob (Farnane et al., 2017), olive stone (Alslaibi et al., 2015) and African palm shell (Moreno-Marenco et al., 2020). In this study, durian *(Duriozibethinus L.)* peel is selected to be converted into activated carbon. Durian is a tropical fruit that can easily found in Malaysia and other Southeast Asia countries. Due to the enormous demand of this fruit especially in Malaysia, the amount of its peel which poses no economic value and creating disposal problems to the community had increased too. Thus, an effort was done in this study to convert the durian peel (DP) into activated carbon to remove MG dye. Physiochemical activation approach comprising of heat treatment together with CO_2 gasification and KOH chemical treatment were employed in this study to create durian peel based AC (DPAC) with good adsorbent characteristic.

EXPERIMENTAL

Materials

Basic dye, MG used in this study as an adsorbate was obtained from Sigma-Aldrich (M) Malaysia. Its chemical formula is $C_{23}H_{26}N_2O \cdot HCl$ and its molecular weight is 382.93 g/mol. Deionized water used to prepare solutions was supplied by USF ELGA water treatment system. The structural formula of MG is given in Fig. 1.
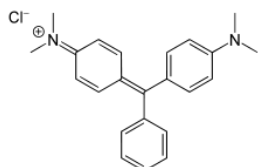

Fig. 1 Chemical structure of MG dye

Synthesis and characterization of DPAC

The DP collected locally in the area of Seberang Jaya, Penang, Malaysia was washed thoroughly to remove dirt on its surfaces. Clean DP was then subjected with dehydrating process at temperature of 110 °C by using an oven (Model Memmert 600, Germany), before being ground and sieved (size of 1-2 mm).

50 g of dried precursor was inserted in the center of the vertical tubular reactor and purging through the reactor was nitrogen gas that flows at 150 cm^3/min. The temperature of the furnace was raise to 550 °C, then held constant for 1 hour. After that, the temperature of the reactor was let to decrease back to room temperature with nitrogen gas purging through the reactor still. The resulted char was collected from the reactor and was impregnated with chemical ativation agent, potassium hydroxide (KOH) at different impregnation ratio (IR), which can be computed using Eq. (1):

$$IR = \frac{w_{KOH}}{w_{char}} \tag{1}$$

where w_{KOH} and w_{char} represent the KOH pellets (dry weight) and char (dry weight), respectively. Char and KOH pellets were mixed together with deionized water using beaker of the size of 250 mL. The mixture was agitated and then kept in oven overnight (110 °C) for dehydrating purposes. Then, the sample was loaded inside the vertical tubular reactor once again, so that the activation step which is quite similar with carbonization process, could take place. This time, nitrogen gas was changed to carbon dioxide (CO_2) once the activation temperature was

reached, at flow rate of 150 cm^3/min and held for certain activation time. The reactor was then allowed to reach room temperature with nitrogen gas purging through it. Hot deionized water together with 0.1 M hydrochloric acid were used to wash the sample in order to recover excess KOH that attached to the sample. The aim in washing step is to obtain pH of washing solution between 6.5 and 7.

Samples was characterized by using surface area analyzer, scanning electron microscopy (SEM), simultaneous thermogravimetric analyzer (STA) and Fourier transform infrared spectroscopy (FTIR). Characterization of DPAC was made in terms of surface area, pore volume and average pore diameter by employing adsorption isotherm of nitrogen at temperature of 77 K by using surface area analyser (Micromeritics, Model ASAP 2020, USA). On the other hand, Brunauer-Emmet-Teller (BET) equation was employed to calculate DPAC's BET surface area. SEM was used to study the surface morphology of the sample. The analysis was carried out using a SEM analyzer (Model Quanta 450 FEG, Netherland). Proximate analysis of the sample was conducted using STA (Model Perkin Elmer STA 6000, USA) whereas the surface chemistry of the sample was measured using FTIR spectroscope (Model IR Prestige 21 Shimadzu, Japan).

Adsorption studies

Batch equilibrium studes for MG-DPAC adsorption system was conducted by focusing on several important parameters namely, effect of MG initial concentration, effect of contact time between adsorbate and adsorbent, effect of MG solution temperature and lastly, effect of MG solution pH. Accurately weighted 1.00 g of MG in powder form was mixed with 1000 mL deionized water to produce 1000 mg/L of stock solution. The sample solution was withdrawn at the point of equilibrium so that the residual concentration can be determined. UV-Visible spectrophotometer (Model Shidmadzu UV-1800, Japan) was used to measure the sample concentration at maximum wavelength of 615 nm. MG dye adsorbed at the point of equilibrium, q_e (mg/g) was computed according to Eq. (2) and MG percetage removal was calculated as expressed in Eq. (3):

$$q_e = \frac{(C_o - C_e)V}{W} \tag{2}$$

$$\% \text{ Removal} = \frac{(C_o - C_e)}{C_o} \times 100\% \tag{3}$$

where C_o and C_e are the MG dye concentration at initial and at equilibrium (mg/g), respectively, V is the volume of MG dye solution (ml) and W is the mass of DPAC (g).

200 mL of adsorbate solutions of pre-determined initial concentratios (25–300 mg/L) were created and filled in six Erlenmeyer flasks with a volume of 250 mL each. The mass of DPAC that was inserted in each flasks containing MG solution was fixed at 0.2 g. The flasks were covered with aluminium foil and loaded in an isothermal water bath shaker. The speed of the rotation for the water bath shaker was fixed at 120 rpm while its temperature was held constant at 30 °C. The process was continue until the MG concentration reading gave an indication that the equilibrium point has been reached. For this particular study, pH of MG solution was not altered.

To study the performance of MG-DPAC system under the influence of temperature, MG solution temperature was change from 30 to 45 and lastly, 60 °C. At these 3 different temperature conditions, parameters namely solution pH, rotating speed and dosage of DPAC were fixed at constant values.

Similarly, the pH of MG solution was change from pH 4 to 10 in order to study the adsorption performance of MG-DPAC system under the influence of pH. The alteration of pH of MG solution was made by the aid of 0.1 M HCl (hydrochloric acid) and/or 0.1 M NaOH (sodium hydroxide) and pH reading was obtained by using pH meter (Model Delta 320, Mettler Toledo, China). The parameters of initial MG concentration, adsorbent dosage and solution temperature were fixed at 50 mg/L, 0.2 g/200 mL and 30 °C, respectively.

In kinetic studies, relatively alike procedure as batch equilibrium studies was performed. However, the sample was taken out for reading

at preset time interval. Quantity of MG dye removed at time t, q_t was computed using the following equation:

$$q_t = \frac{(C_o - C_t)V}{W} \qquad (4)$$

where C_o and C_t are the MG dye concentration at initial and at time t (mg/g), respectively, V is the volume of MG dye solution (ml) and W is the mass of DPAC (g). The normalized standard deviation Δq_t (%) for validation of kinetic model was calculated using (Weng et al., 2009):

$$\Delta q_t (\%) = 100 \sqrt{\frac{\sum[(q_{t,exp} - q_{t,cal})/q_{t,exp}]^2}{(n-1)}} \qquad (5)$$

where n is data points while measured MG and calculated MG adsorbed at time t were denoted by $q_{t,exp}$ and $q_{t,cal}$, respectively.

RESULTS AND DISCUSSION

Characteristics of samples

The values of surface area (BET and mesopores) and pore characteristics (volume and diameter) for DP, DP char and DPAC were tabulated in Table 1. The surface area for DPAC was 886.31 m²/g whereas the surface area for DP was not available since there was no pore identified. Surface area obtained was considered average compared to ACs derived from Egyptian wood of 603 m²/g (Ilnicka et al., 2020), durian seed of 980.62 m²/g (Ab Razak et al., 2015) and spent mushroom compost of 1419.11 m²/g (Karadirek and Okkay, 2018). The average pore diameter for DPAC was 2.57 nm which belong to mesopores region according to the IUPAC classification. KOH impregnation and CO_2 gasification applied during the activation steps had developed new pores and widening existing pores thus contributing to the surface area enhancement in DPAC. Dehydration of KOH produced K_2O which subsequently reacted with CO_2 to yield K_2CO_3. K_2CO_3 was mobile and penetrated deep into the DPAC's skeleton and causing an increase to both surface area and pore volume.

Table 1 Surface area and pore characteristics of samples.

Sample	BET surface area (m²/g)	Mesopore surface area (m²/g)	Total pore volume (cm³/g)	Average pore diameter (nm)
DP	2.07	-	-	-
DP char	177.64	85.68	0.17	2.49
DPAC	886.31	547.85	0.50	2.57

Fig. 2 provides the morphology of DP and DPAC. The surface of DP (Fig. 2(a)) was rough with minimal existence of small size of pores. The surface of DPAC (Fig. 2(b)) was observed to be highly porous with cavities scattered irregularly across the whole surface. These heterogeneous cavities were resulted from the evaporation of impregnated KOH-derived compounds. Combination of CO_2 and KOH treatments were succeeded in aiding the well-development of pores on DPAC's surface.
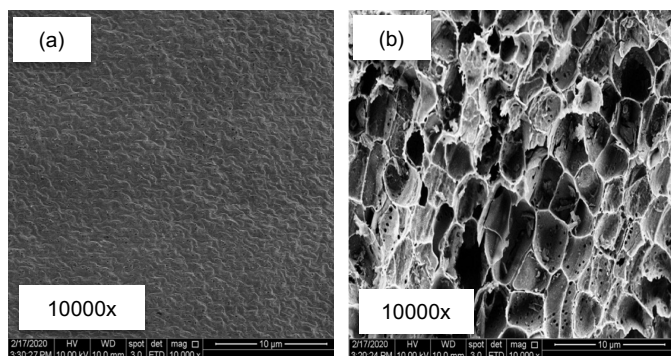

Fig. 2 SEM images of (a) DP and (b) DPAC.

Proximate analysis for samples is tabulated in Table 2. DP contains 20.69 % of fixed carbon which can be considered moderate and suitable to be converted to AC at the first place. Other agricultural wastes contained wide range of fixed carbon from 11 % of kenaf fiber (Shamsuddin et al., 2016) to 34.80 % of orange peel (Lam et al., 2017). After activation processes, DPAC showed a significant increase in fixed carbon and a drastic decreased in volatile composition. At high activation temperature, most of the volatile and moisture were removed from the sample and leave behind high carbon content.

Table 2 Proximate analysis of samples.

Sample	Proximate analysis (%)			
	Moisture	Volatile	Fixed carbon	Ash
DP	12.70	65.22	20.69	1.39
DP char	4.81	37.81	55.80	1.58
DPAC	1.54	23.60	73.20	1.66

The surface chemistry of DP and DPAC is given in Fig. 3. It was observed that DP was having bandwidth at 3233 and 3459 cm⁻¹ (O-H functional group) (Ghaedi et al., 2015), 2351 cm⁻¹ (C≡C stretching of alkyne group) (Georgin et al., 2016), 1647 cm⁻¹ (C=C alkene group) (Zhou et al., 2017), 1420 and 1498 cm⁻¹ (C-O stretching of ether) (Kumar and Jena, 2016), 1053 cm⁻¹ (carboxylic acid or ester group) (Gautam et al., 2015) and 616-825 cm⁻¹ (C-H out of plane bonding in benzene derivatives) (Lin et al., 2017). The surface chemistry of the DPAC was contradicted from its precursor since several functional groups had shifted or disappeared after the activation processes. Spectrum of DPAC shows that a few peaks located in the region of 2351 cm⁻¹ (C≡C alkyne group) and 1647 cm⁻¹ (C=C alkene group) were diminished. It was noticed that the peaks in the region of 614-827 cm⁻¹ which signified C-H out-of-plane bonding in benzene derivatives for DPAC was disappeared. Aromatic group diminished because of oxidative breakdown of benzene during pyrolysis and activation processes.
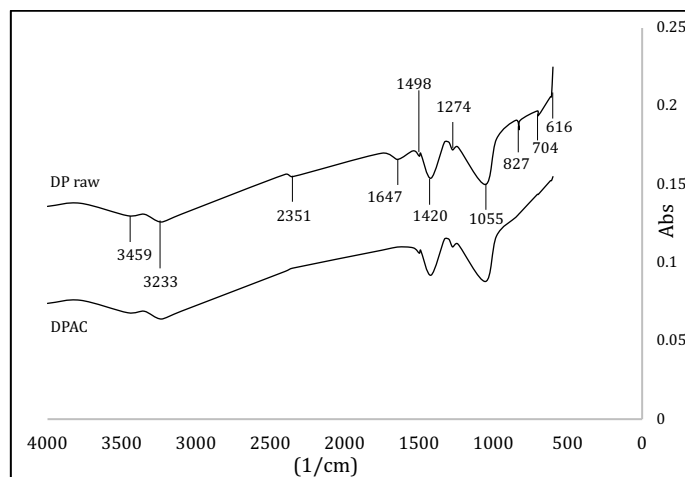
Fig. 3 FTIR spectrums for DP and DPAC.

Batch equililrium studies

Figs. 4 and 5 show the MG adsorption uptake and MG removal by DPAC at 30 °C, respectively. In the beginning, DPAC has excess surface sites which were available for the adsorption to occur. The amount of MG adsorbed together with the MG removal were found to rise with time until reached the equilibrium point. This point indicated that DPAC had became saturated, thus no more MG dye can be adsorbed. Plus, the repulsion that occur between MG dye in solid phase and bulk phase increase the difficulty of the remaining active sites on DPAC to be filled by MG dye. MG adsorption uptakes by DPAC was noticed to rise from 23.50 to 211.32 mg/g as the MG dye initial concentration increased from 25 to 300 mg/L. This was due to the occurrence of larger mass transfer driving force for higher MG

concentration, resulted in higher MG uptake. However, as the initial concentration of adsorbate was altered from 25 to 300 mg/L, the removal of MG decreased. The MG removal of higher than 84 % was obtained for low initial concentration (25 to 100 mg/L) as the ratio of initial number of dye molecules to the accessible surface area was high.
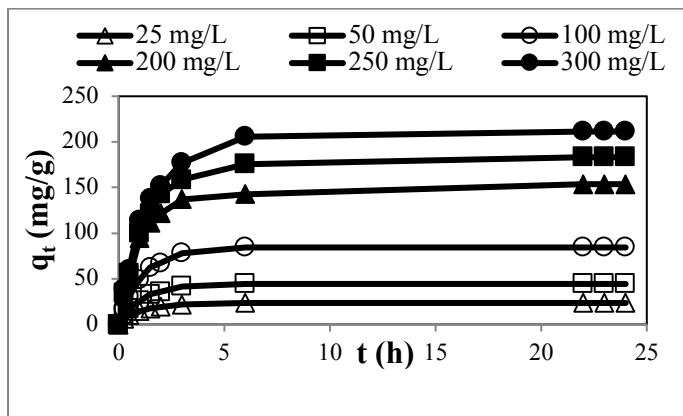

Fig. 4 MG adsorption uptake by DPAC versus the time at 30°C.
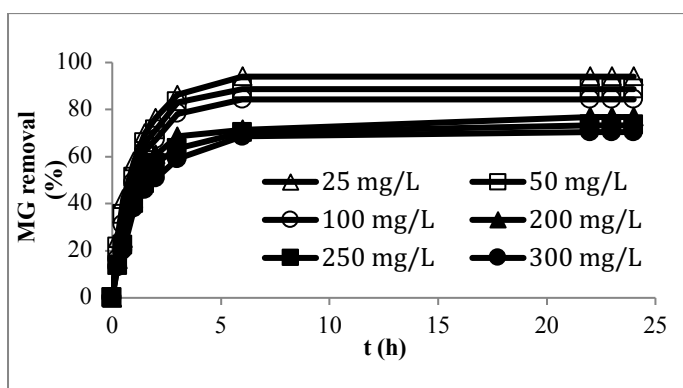

Fig. 5 MG percent removal by DPAC versus the time at 30°C.

Longer contact time was needed by the MG solution to attain equilibrium for higher MG initial concentration. For the lower initial concentrations (25 to 100 mg/L), DPAC required 4 to 5 hours whereas for higher initial concentrations (200 to 300 mg/L), 22 to 24 hours was required to reach equilibrium.

The impact of solution temperature on MG adsorption by the DPAC is shown in Fig. 6. Adsorption of MG dye onto DPAC showed an exothermic nature where the adsorption uptakes were decreased as the solution temperature increased (Eltaweil et al., 2020). The decreasing trend in MG adsorption uptakes when temperature was increased was expected to be caused by the intensification of desorption step in the sorption mechanis (Doumic et al., 2015). This phenomenon was also contributed by the decrease in intensity of sorptive forces that occurred in MG-DPAC adsorption system.
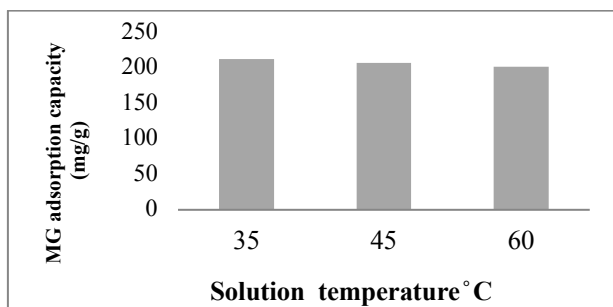

Fig. 6 MG removal by DPAC at different solution temperature.

Fig. 7 illustrates the influence of initial pH on the MG adsorption by DPAC. The MG removal by DPAC was increased as the pH increased from 4 to 8. The highest removal was obtained at pH 8 of 90.63 %, which proved that the MG adsorption was favor at alkaline condition. At acidic condition, the removal was low due to the existence of extra hydrogen ions competed with the MG ions for adsorption (Shakib et al., 2017). At higher pH, active sites with negative charge increased while active sites with positive charge decreased. This diminished the electrostatic repulsion between DPAC's active sites and MG positive ions, thus resulted in an increased of MG adsorption uptakes.
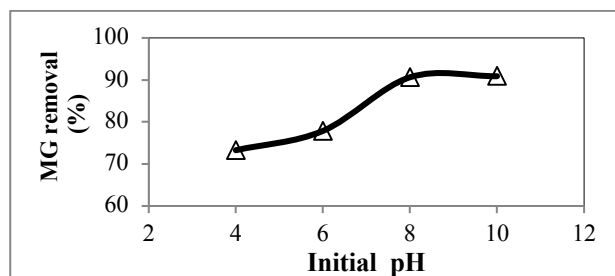

Fig. 7 MG removal by DPAC at different solution pH.

Isotherms studies provide valuable information about the relationship between adsorbate molecules in bulk phase and solid phase. In this study, eight isotherms were employed namely Langmuir, Freundlich, Temkin, Dubinin-Radushkevich (DR), Koble-Corrigan (KC), Vieth-Sladek (VS), Sips and Brouers-Sotolongo (BS).

Langmuir isotherm was developed by assuming the adsorbate formed a monolayer coverage on adsorbent's surface. One of the most vital information can be obtained from this isotherm is the Langmuir monolayer adsorption capacity. The following equation gave the linear form of Langmuir isotherm (Langmuir, 1918):

$$\frac{C_e}{q_e} = \frac{C_e}{q_m} + \frac{1}{K_L q_m} \qquad (6)$$

where q_e is the quantity of MG dye removed at equilibrium (mg/g), q_m is the monolayer adsorption capacity (mg/g), C_e is the MG dye concentration at equilibrium (mg/L) and K_L is the Langmuir adsorption constant (L/mg).

Freundlich isotherm was developed by assuming that the adsorbate formed a multilayer coverage on adsorbent's heterogeneous surface and its linear form was expressed as follows (Freundlich, 1906):

$$\log q_e = \frac{1}{n_F} \log C_e + \log K_F \qquad (7)$$

where q_e is the quantity of MG dye removed at equilibrium (mg/g), C_e is the MG dye concentration at equilibrium (mg/L), K_F is the Freundlich adsorption constant (mg/g)(L/mg)$^{1/n}$ and n_F is the heterogeneity factor.

The equation of Temkin isotherm was built by considering the effect of uniformly distributed binding energies between adsorbent and adsorbate. It is assumed that the heat of adsorption would dropped linearly with adsorbate's coverage on adsorbent. Simplified linear equation of Temkin isotherm is expressed as follows (Temkin and Pyzhev, 1940):

$$q_e = B_T \ln A_T + B_T \ln C_e \qquad (8)$$

where q_e is the quantity of MG dye removed at equilibrium (mg/g), C_e is the MG dye concentration at equilibrium (mg/L), T is the absolute temperature (K), R is the universal gas constant (8.314 J/mol.K), A_T is the equilibrium binding constant (L/mg) and B_T is the constant which related to the adsorption heat (L/mg).

DR isotherm estimates the characteristic porosity of the adsorbent, plus with adsorption's apparent energy. When the free energy, E_{DR}

obtained is in between of 8 and 16 kJ/mol, it signifies chemisorption. On the other hand, the value that below 8 kJ/mol inidcates physisorption process. The equation of DR isotherm is expressed as follows (Dubinin and Radushkevich, 1947):

$$q_e = q_m e^{-\beta \varepsilon^2} \tag{9}$$

$$\varepsilon = RT \ln\left[1 + \frac{1}{C_e}\right] \tag{10}$$

Free energy E_{DR} of sorption was calculated as follows:

$$E_{DR} = \frac{1}{\sqrt{2B_{DR}}} \tag{11}$$

where q_e is the quantity of MG dye removed at equilibrium (mg/g), q_m is the monolayer adsorption capacity (mg/g), C_e is the MG dye concentration at equilibrium (mg/L), T is absolute temperature (K), R is the universal gas constant (8.314 J/mol K) and B_{DR} is DR constant.

Isotherm model of Koble-Corrigan (KC) is an empirical model with 3 parameters. This model is given by following equation (Koble and Corrigan, 1952):

$$q_e = \frac{a_{KC} C_e^{n_{KC}}}{1 + b_{KC} C_e^{n_{KC}}} \tag{12}$$

where q_e is the quantity of MG dye removed at equilibrium (mg/g), C_e is the MG dye concentration at equilibrium (mg/L) and a_{KC}, b_{KC} and n_{KC} are the KC parameters. If the value of parameter n_{KC} is close to 1, it signifies that the isotherm is becoming more of Langmuir isotherm.

The Vieth-Sladek (VS) isotherm equation is expressed as follows (Vieth and Sladek, 1965):

$$q_e = k_{VS} C_e + \frac{q_m \beta_{VS} C_e}{1 + \beta_{VS} C_e} \tag{13}$$

where q_e is the quantity of MG dye removed at equilibrium (mg/g), q_m is the monolayer adsorption capacity (mg/g), C_e is the MG dye concentration at equilibrium (mg/L) and k_{VS} and β_{VS} are VS constants.

Sips isotherm equation is given as (Sips, 1948):

$$q_e = \frac{q_m (k_s C_e)^{m_S}}{1 + (k_s C_e)^{m_S}} \tag{14}$$

where q_e is the quantity of MG dye removed at equilibrium (mg/g) and C_e is the MG dye concentration at equilibrium (mg/L) and q_m, m_S, k_S and n_S are Sips parameters. When m_S equals to unity, the Sips isotherm becomes Langmuir isotherm. On the other hand, deviation of m_S value from unity indicates heterogenous surface.

The Brouers-Sotolongo (BS) isotherm is given by (Gregg and Sing, 1967):

$$q_e = q_m \left(1 - e^{-k_{BS} C_e^{\alpha}}\right) \tag{15}$$

where q_e is the quantity of MG dye removed at equilibrium (mg/g), C_e is the MG dye concentration at equilibrium (mg/L) and k_{BS}, α and q_m are BS parameters. The parameters q_m, k_{BS} and α can be determined by a non-linear curve fitting procedure. The exponent signifies the energy heterogeneity of the surface of adsorbent.

The summary of the isotherm constants for MG-DPAC adsorption system were given in Table 3. Comparison on R^2 values revealed that adsorption data matched the isotherm models in the sequence of Freundlich > Langmuir > Temkin > KC > BS > Sips > VS > DR. Freundlich isotherm fitted well with the data ($R^2 > 0.99$), which signifies that a multilayer sorption was occurred at DPAC's heterogenous surface. The values of n_F was 3.06 which indicative of high adsorption intensity (Tunc et al., 2009). The heterogeneity in the surface of the DPAC significantly affect the MG adsorption. The high K_F values of 19.08 indicate the higher adsorption capacity. Freundlich isotherm was preferred by other studies of basic blue removal by pineapple plant stem based AC (Chan et al., 2016). The maximum

monolayer capacity, q_m values from the models obtained were in range 231.17 to 241.66 mg/g.

Table 3 Parameters of isotherms.

Langmuir	Freundlich	Temkin	Dubinin-Radushkevich
q_m = 231.17	K_F =19.08	B_T = 46.73	E_{DR} = 2236.07
k_L = 0.11	n_F = 3.06	A_T = 0.06	B_{DR} = 0.0070
R^2 = 0.98	R^2 = 0.99	R^2 = 0.94	R^2 = 0.72
Koble-Corrigan	**Vieth-Sladek**	**Brouers-Sotolongo**	**Sips**
a_{KC}= 38.13	k_{VS} = 0.96	q_m = 243.33	q_m = 245.85
b_{KC} = 0.0010	q_m = 241.66	k_{BS} = 0.030	k_S = 0.00012
n_{KC} = 0.34	β_{VS} = 1.05	α = 0.35	m_S= 0.37
R^2 = 0.90	R^2 = 0.89	R^2 = 0.90	R^2 = 0.89

Additional analysis of the Langmuir isotherm can be computed by using the following equation to find separation factor, R_L:

$$R_L = \frac{1}{1 + K_L C_o} \tag{16}$$

where C_o is the initial concentration of MG dye (mg/L). Different value of R_L indicates different condition: $0 < R_L < 1$ indicates favourable adsorption, $R_L > 1$ indicates unfavourable adsorption, $R_L = 1$ indicates linear adsorption and $R_L = 0$ indicates irreversible adsorption. Fig. 8 shows the graph of the R_L versus MG initial concentrations. From Fig. 9, it can be seen that R_L values obtained were in favorable region. As the initial concentration rises from 25 to 300 mg/L, a gradual drop of R_L was spotted, which signified that adsorption process at higher initial MG dye concentration was preferred.
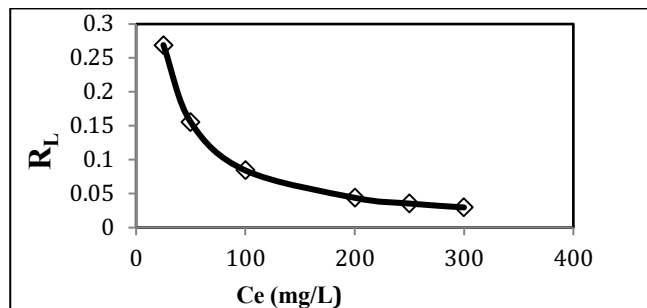
Fig. 8 Plots of separation factor for different initial concentration.

Adsorption kinetics

Kinetic studies provides the rate of reaction for adsorption process. This study employed 4 kinetic models namely, pseudo-first-order (PFO) model, pseudo-second-order (PSO) model, Elovich model and Avrami model.

The pseudo-first-order (PFO) model is given as (Lagergen and Svenska, 1898):

$$\ln(q_e - q_t) = \ln q_e - k_1 t \tag{17}$$

where q_e and q_t are the quantity of MG dye removed at equilibrium and at time t (mg/g), respectively, k_1 is the rate constant for PFO model (1/min) and t is time (min).

Equation for pseudo-second-order (PSO) model is given as follows (Ho and Mckay, 1999):

$$\frac{t}{q_t} = \frac{1}{q_e^2 k_2} + \frac{1}{q_e} t \tag{18}$$

where q_e and q_t are the quantity of MG dye removed at equilibrium and at time t (mg/g), respectively, k_2 is the rate constant for PSO model (g/mg h) and t is time (min).

Equation of Elovich kinetic model is as follows (Aharoni and Tompkins, 1970):

$$q_t = \frac{1}{B_E}\ln(A_E B_E) + \frac{1}{B_E}\ln(t) \qquad (19)$$

where q_t is the MG dye adsorbed at time t (mg/g), A is the rate of initial sorption (mg/g h), B is the parameter related to surface coverage extension (g/mg) and $1/B_E$ reflects the number of sites available for adsorption.

Avrami kinetic model is given as (Putniss, 1995):

$$q_t = q_e(1 - \exp(-k_{AV}t)^{n_{AV}}) \qquad (20)$$

In simpler form, this equation becomes:

$$\alpha_t = (1 - \exp(-k_{AV}t)^{n_{AV}}) \qquad (21)$$

The linearized form of this equation is:

$$\ln(-\ln(1 - \alpha_t)) = n_{AV}\ln k_{AV} + n_{AV}\ln t \qquad (22)$$

where q_e and q_t are the quantity of MG dye removed at equilibrium and at time t (mg/g), respectively, k_{AV} is the Avrami kinetic constant, n_{AV} is the constant that reflects the adsorption mechanism changes and α_t is the adsorption fraction of q_t/q_e. Table 4 shows the kinetic parameters for the MG adsorption onto DPAC. Based on Table 4, PFO kinetic model was revealed to match the data the best as shown by the highest R^2 values with small standard deviation, Δq_t. Furthermore, the values of q_e calculated using PFO equation is comparable to those obtained from the experiment which resulted Δq_t to be ranging from 0.69 to 8.50 %. There were consistent decreasing trends in the k_1 values obtained with the increasing of MG initial concentrations. A low adsorption rate was noticed at higher MG dye concentration owing to the highly competitive of MG dye to compete for DPAC's active sites.

Table 4 Kinetic parameters for MG adsorption onto DPAC.

		MG initial concentration (mg/L)					
		25	50	100	200	250	300
P F O	q_e, exp (mg/g)	24.70	48.68	86.23	144.29	168.13	186.42
	q_e, cal (mg/g)	23.35	44.54	85.63	138.40	163.69	172.43
	k_1	0.85	0.70	0.53	0.51	0.49	0.47
	R^2	0.99	0.98	0.99	0.95	0.97	0.96
	Δq_t (%)	5.47	8.50	0.69	4.08	2.64	7.50
P S O	q_e, cal (mg/g)	37.04	71.43	142.86	225.56	275.72	313.42
	k_2	0.017	0.0085	0.0023	0.00028	0.00029	0.00030
	R^2	0.91	0.91	0.98	0.84	0.60	0.64
	Δq_t (%)	49.96	46.73	65.67	56.32	63.99	68.13
E l o v i c h	q_e, cal (mg/g)	27.00	52.85	91.64	156.21	179.55	199.97
	A_E	10.27	3.66	0.61	0.35	0.21	0.20
	B_E	3.93	8.05	16.69	28.56	34.71	38.49
	R^2	0.82	0.86	0.94	0.91	0.93	0.92
	Δq_t (%)	9.31	8.57	6.27	8.26	6.80	7.27
A v r a m i	q_e, cal (mg/g)	23.29	45.54	80.01	122.33	135.64	154.30
	k_{AV}	0.011	0.0095	0.0055	0.0057	0.0047	0.0049
	n_{AV}	0.50	0.52	0.62	0.65	0.69	0.69
	R^2	0.61	0.66	0.78	0.75	0.79	0.78
	Δq_t (%)	5.71	6.45	7.21	15.22	19.32	17.23

The mechanism of MG diffusion was investigated by using Intraparticle diffusion and Boyd models. Intraparticle diffusion model is usual to majority of adsorption process where the uptake of adsorbate differs nearly proportional with $t^{1/2}$. The equation of this model expressed as (Weber and Morris, 1962):

$$q_t = k_{dif}t^{1/2} + C \qquad (23)$$

where q_t is the quantity of MG dye removed at time t (mg/g), k_{diff} is the rate constant (mg/g h$^{1/2}$) and C is the boundary layer thickness. Fig. 9 shows the plot of intraparticle diffusion for MG-DPAC adsorption system for various MG initial concentrations. This plot formed a multi-linear lines with three distinctive sections. The first sharper section represents the external mass transfer which completed within 15 minutes owing to powerful electrostatic attraction betwixt MG dye and DPAC's external surface.
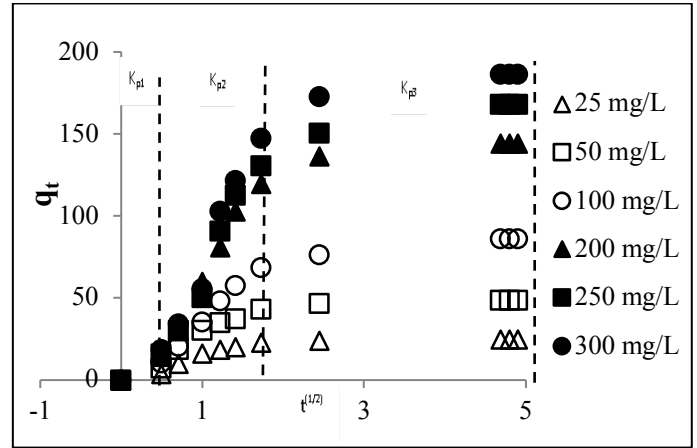
Fig. 9 Intraparticle diffusion plot for MG adsorption onto DPAC.

The next section where the rate limiting step is caused by intraparticle diffusion is known as gradual adsorption. The third section which is known as final equilibrium stage signifies a drop in intraparticle diffusion because of exceptionally low MG dye concentration left in the solution. It can be concluded that intraparticle diffusion was not the only rate-limiting step in the second and third sections since the linear lines do not pass through the origin. Table 5 tabulates the values of the intraparticle diffusion model constants (k_{pi} and C_i) for the three regions from the plots of q_t versus $t^{1/2}$ together with the R^2 values. From Table 5, it can be seen that k_{pi} for all sections increased with the increased of initial dye concentrations. The explanation behind this is that an increasing in adsorbate concentration caused the driving force to increase, thus lead to an increase in the MG diffusion rate. Besides k_{pi}, C_i was also found to increase as the MG initial concentrations increase which indicates an increase of the boundary layer thickness and increase of the chance of internal mass transfer (Marrakchi et al., 2017).

Boyd kinetic model is applied to decide the slowest step in the adsorption process, as described in (Boyd et al., 1947):

$$B_t = -0.4977 - \ln\left(1 - \frac{q_t}{q_e}\right) \qquad (24)$$

where q_e and q_t are the quantity of MG dye removed at equilibrium and at time t (mg/g), respectively. Fig. 10 illustrates the Boyd plots and from the plot, the linear lines did not passing through the origin, for all MG initial concentrations. Therefore, it can be said that the adsorption of MG dye onto DPAC was mainly regulated by the processes that were managed by film diffusion.

Thermodynamic studies

Three important parameters in thermodynamic studies; enthalpy of adsorption ($\Delta H°$), free energy ($\Delta G°$) and entropy ($\Delta S°$) were discovered and given in Table 5 together with activation energy value, E_a. The value of $\Delta H°$ and $\Delta S°$ can be obtained from equation given below:

$$\ln K_L = \frac{\Delta S°}{R} - \frac{\Delta H°}{RT} \qquad (25)$$

The next following equation can be applied to obtain the value of $\Delta G°$ is:

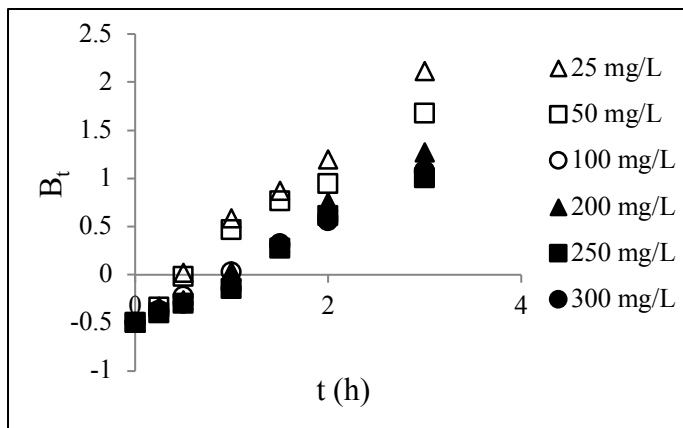$$\Delta G° = -RT\ln K_L \qquad (26)$$

Fig. 10 Boyd plot for MG adsorption onto DPAC.

where R is the universal gas constant (8.314 J/mol K), T is absolute solution temperature (K) and K_L is the Langmuir isotherm constant (L/mg). Activation energy of adsorption refers to the lowest energy which is required by reactant for the reaction to progress. This energy can be determined by employing Arrhenius equation which is given as follows:

$$\ln k_2 = \ln A - \frac{E_a}{RT} \qquad (27)$$

where k_2 is the rate constant of PSO model (g/mg h), E_a is the Arrhenius activation energy of adsorption (kJ/mol), A is the Arrhenius factor, R is the universal gas constant (8.314 J/mol K) and T is the absolute temperature (K). From Table 5, negative value of $\Delta H°$ signified nature of exothermic process. This result was in agreement with those results obtained in effect of solution temperature section in 3.3. Exothermic nature occurs due to the fact that physical bonding between MG dye and DPAC's active sites got reduced as temperature increased. Apart from that, solubility of MG dye was enhanced owing to a greater interaction forces between MG dye and water as compared to a weaker interaction forces between MG dye and DPAC, hence the solute was more difficult to be adsorbed. Exothermic nature can be observed in the studies of Basic Blue 3 adsorption onto pineapple plant stem based AC (Chan et al., 2016). The negative value of $\Delta S°$, suggest the decrease in adsorbate concentration in solid-liquid interface, which signified that there is an increase in adsorbate concentration onto the solid phase. It can also be deduced that the randomness at the solid-liquid interface had decreased during adsorption process. This phenomenon is common for physical-type of adsorption where the adsorption process was driven by electrostatic interaction.

Low activation energy between 5–40 kJ/mol indicates physical adsorption. On contrary, energy between 40–800 kJ/mol proposes chemisorption. Activation energy, E_a for MG-DPAC system was found to be positive and below than 40 kJ/mol, thus indicated that the rate limiting step was physically control type. $\Delta G°$ with negative values as obtained in this study signified that MG-DPAC adsorption process had a spontaneous and feasible nature. Table 6 shows the summary of other AC adsorbents in adsorbing MG dye.

Table 5 Thermodynamic parameters for MG adsorption onto DPAC.

ΔH° (kJ/mol)	ΔS° (J/mol)	Eₐ (kJ/mol)	ΔG° (kJ/mol)		
			303K	318K	333K
-30.15	-0.12	29.94	-1.19	-0.73	-0.28

CONCLUSION

In this study, the adsorption of MG dye onto DPAC was increased with the increase of contact time and dye initial concentration. The adsorption system poses exothermic nature as the adsorption uptakes was decreased as the solution temperature increased. pH 8 was found to be the optimum pH for the MG dye adsorption onto DPAC. Isotherm and kinetic studies revealed that Freundlich isotherm and PFO kinetic model fit the data the best. Further analysis using Boyd plot confirmed that adsorption of MG onto DPAC was mainly governed by the film diffusion controlled mechanism. Thermodynamic studies revealed low value of activation energy, E_a which indicates that the rate-limiting step in MG adsorption was physically control type. DPAC was found to be suitable to remove MG dye from aqueous solution due to high maximum adsorption capacity that it poses.

Table 6 Summary of other AC adsorbents in adsorbing MG dye.

Precursor	Adsorption capacity (mg/g)	Isotherm	Kinetic	Thermodynamic	References
Durian peel	231.17	Freundlich	PFO	Exothermic	This study
Pinus roxburghii cone	250.00	Langmuir	PSO	-	(Sharma et al., 2019)
Apple seed	706.72	Liu	General order model	Exothermic	(Adebayo et al., 2020)
Lichen *Cetraria islandica*	666.22	Freundlich	PSO	Endothermic	(Koyuncu and Kul, 2020)
Spent grain	2.55	Langmuir	PSO	Exothermic	(Chanzu et al., 2019)
Walnut shell	11.76	Langmuir	PSO	-	(Hajialigol and Masoum, 2019)
Coffee husk	263.00	Sips	PSO	Endothermic	(Krishna Murthy et al., 2019)
Luffa aegyptica peel	78.79	Langmuir	PSO	Endothermic	(Mashkoor and Nasar, 2019)
Chrysopogon zizanioides roots	128.10	Freundlich	PSO	-	(Thanarasu et al., 2020)

REFERENCES

Ab Razak, N. H., Praveena, S. M., Aris, A. Z., Hashim, Z. 2015. Drinking water studies: A review on heavy metal, application of biomarker and health risk assessment (A Special Focus In Malaysia). *J. Epidemiol. Glob. Health,* 5, 297-310.

Adebayo, M. A., Adebomi, J. I., Abe, T. O., Areo, F. I. 2020. Removal of aqueous congo red and malachite green using ackee apple seed–bentonite composite. *Colloid Interface. Sci. Commun.,* 38, 100311.

Aderemi, H. B., Nasri, N. S., Zainia, M. A. A. 2018. Physicochemical properties of char derived from palm fatty acid distillate. *Mal. J. Fund. Appl. Sci.,* 14, 403-406.

Aharoni, C., Tompkins, F. C. 1970. Advances in catalysis and related subjects. *Academic Press,* 31.

Ahmad, M. A., Ahmad, N., Bello, O. S. 2015. Adsorption kinetic studies for the removal of synthetic dye using durian seed activated carbon. *J. Dispers. Sci. Technol.,* 36, 670-684.

Alslaibi, T. M., Abustan, I., Ahmad, M. A., Abu Foul, A. 2015. Comparative studies on the olive stone activated carbon adsorption of Zn^{2+}, Ni^{2+}, and Cd^{2+} from synthetic wastewater. *Desalination Water Treat.,* 54, 166-177.

Ayanda, O. S., Amodu, O. S., Adubiaro, H., Olutona, G. O., Ebenezer, O. T., Nelana, S. M., Naidoo, E. B. 2018. Effectiveness of termite hill as an economic adsorbent for the adsorption of alizarin red dye. *J. Water Reuse Desalination,* 9, 83-93.

Aziz, N. S. M., Shariff, A., Abdullah, N., Noor, N. M. 2018. Characteristics of coconut frond as a potential feedstock for biochar via slow pyrolysis. *Mal. J. Fund. Appl. Sci.,* 14, 408-413.

Bahadori, E., Rapf, M., Di Michele, A., Rossetti, I. 2020. Photochemical vs photocatalytic azo-dye removal in a pilot free-surface reactor: is the catalyst effective? *Sep. Purif. Technol.,* 237, 116320.

Bai, Y.-N., Wang, X.-N., Zhang, F., Wu, J., Zhang, W., Lu, Y.-Z., Fu, L., Lau, T.-C., Zeng, R. J. 2020. High-rate anaerobic decolorization of methyl orange

from synthetic azo dye wastewater in a methane-based hollow fiber membrane bioreactor. *J. Hazard. Mater.,* 388, 121753.

Berkessa, Y. W., Yan, B., Li, T., Jegatheesan, V., Zhang, Y. 2020. Treatment of anthraquinone dye textile wastewater using anaerobic dynamic membrane bioreactor: performance and microbial dynamics. *Chemosphere,* 238, 124539.

Bhatti, H. N., Jabeen, A., Iqbal, M., Noreen, S., Naseem, Z. 2017. Adsorptive behavior of rice bran-based composites for malachite green dye: isotherm, kinetic and thermodynamic studies. *J. Mol. Liq.,* 237, 322-333.

Boyd, G. E., Adamson, A. W., Myers, L. S. 1947. The exchange adsorption of ions from aqueous solutions by organic zeolites II. *J. Am. Chem. Soc.,* 69, 11, 2836-2848.

Chan, S.-L., Tan, Y. P., Abdullah, A. H., Ong, S.-T. 2016. Equilibrium, kinetic and thermodynamic studies of a new potential biosorbent for the removal of basic blue 3 and congo red dyes: pineapple (*ananas comosus*) plant stem. *J. Taiwan Inst. Chem. Eng.,* 61, 306-315.

Chanzu, H. A., Onyari, J. M., Shiundu, P. M. 2019. Brewers' spent grain in adsorption of aqueous congo red and malachite green dyes: batch and continuous flow systems. *J. Hazard. Mater.,* 380, 120897.

Doumic, L., Salierno, G., Cassanello, M., Haure, P., Ayude, M. 2015. Efficient removal of orange g using prussian blue nanoparticles supported over alumina. *Catal. Today,* 240, 67-72.

Dubinin, M. M., Radushkevich, L. V. 1947. The equation of the characteristic curve of activated charcoal. *Proc. USSR Acad. Sci.; Physical Chemisty Section,* 55, 331-337.

Eltaweil, A. S., Elgarhy, G. S., El-Subruiti, G. M., Omer, A. M. 2020. Carboxymethyl cellulose/carboxylated graphene oxide composite microbeads for efficient adsorption of cationic methylene blue dye. *Int. J. Biol. Macromol.,* 154, 307-318.

Farnane, M., Tounsadi, H., Machrouhi, A., Elhalil, A., Mahjoubi, F. Z., Sadiq, M., Abdennouri, M., Qourzal, S., Barka, N. 2017. Dye removal from aqueous solution by raw maize corncob and H_3PO_4 activated maize corncob. *J. Water Reuse Desalination,* 8, 214-224.

Freundlich, H. M. F. 1906. Over the adsorption in solution. *J. Phys. Chem.,* 57, 385-471.

Gautam, R. K., Gautam, P. K., Banerjee, S., Rawat, V., Soni, S., Sharma, S. K., Chattopadhyaya, M. C. 2015. Removal of tartrazine by activated carbon biosorbents of *lantana camara*: kinetics, equilibrium modeling and spectroscopic analysis. *J. Environ. Chem. Eng.,* 3, 79-88.

Georgin, J., Dotto, G. L., Mazutti, M. A., Foletto, E. L. 2016. Preparation of activated carbon from peanut shell by conventional pyrolysis and microwave irradiation-pyrolysis to remove organic dyes from aqueous solutions. *J. Environ. Chem. Eng.,* 4, 266-275.

Ghaedi, M., Nasab, A. G., Khodadoust, S., Sahraei, R., Daneshfar, A. 2015. Characterization of zinc oxide nanorods loaded on activated carbon as cheap and efficient adsorbent for removal of methylene blue. *J. Ind. Eng. Chem.,* 21, 986-993.

Gregg, S. J., Sing, K. S. W. 1967. Adsorption, surface area and porosity. *New York: Academic Press*, 208.

Hajialigol, S., Masoum, S. 2019. Optimization of biosorption potential of nano biomass derived from walnut shell for the removal of malachite green from liquids solution: experimental design approaches. *J. Mol. Liq.,* 286, 110904.

Ho, Y. S., Mckay, G. 1999. Sorption of dye from aqueous solution by peat. *Chem. Eng. J.,* 70, 115-124.

Ilnicka, A., Kamedulski, P., Aly, H. M., Lukaszewicz, J. P. 2020. Manufacture of activated carbons using Egyptian wood resources and its application in oligothiophene dye adsorption. *Arab. J. Chem.,* 13, 5284-5291.

Karadirek, Ş., Okkay, H. 2018. Statistical modeling of activated carbon production from spent mushroom compost. *J. Ind. Eng. Chem.,* 63, 340-347.

Khouni, I., Louhichi, G., Ghrabi, A. 2020. Assessing the performances of an aerobic membrane bioreactor for textile wastewater treatment: influence of dye mass loading rate and biomass concentration. *Process Saf. Environ. Prot.,* 135, 364-382.

Koble, R. A., Corrigan, T. E. 1952. Adsorption isotherm for pure hydrocarbons. *Ind. Eng. Chem.,* 44, 383-387.

Koyuncu, H., Kul, A. R. 2020. Synthesis and characterization of a novel activated carbon using nonliving lichen *cetraria islandica (l.) ach.* and its application in water remediation: equilibrium, kinetic and thermodynamic studies of malachite green removal from aqueous media. *Surf. Interfaces,* 21, 100653.

Krishna Murthy, T. P., Gowrishankar, B. S., Chandra Prabha, M. N., Kruthi, M., Hari Krishna, R. 2019. Studies on batch adsorptive removal of malachite green from synthetic wastewater using acid treated coffee husk: equilibrium, kinetics and thermodynamic studies. *Microchem. J.,* 146, 192-201.

Kumar, A., Jena, H. M. 2016. Preparation and characterization of high surface area activated carbon from fox nut (*euryale ferox*) shell by chemical activation with H_3PO_4. *Results Phys.,* 6, 651-658.

Lagergen, S., Svenska, K. 1898. About the theory of so-called adsorption of soluble substances. *Acta Holmensia,* 24, 1-39.

Lam, S. S., Liew, R. K., Wong, Y. M., Yek, P. N. Y., Ma, N. L., Lee, C. L., Chase, H. A. 2017. Microwave-assisted pyrolysis with chemical activation, an innovative method to convert orange peel into activated carbon with improved properties as dye adsorbent. *J. Clean. Prod.,* 162, 1376-1387.

Langmuir, I. 1918. The adsorption of gases on plane surfaces of glass, mica and platinum. *J. Am. Chem. Soc.,* 40, 1361.

Lin, Q., Gao, M., Chang, J., Ma, H. 2017. Highly effective adsorption performance of carboxymethyl cellulose microspheres crosslinked with epichlorohydrin. *J. Appl. Polym. Sci.,* 2, 134.

Machrouhi, A., Farnane, M., Elhalil, A., Elmoubarki, R., Abdennouri, M., Qourzal, S., Tounsadi, H., Barka, N. 2017. Effectiveness of beetroot seeds and H_3PO_4 activated beetroot seeds for the removal of dyes from aqueous solutions. *J. Water Reuse Desalination,* 8, 522-531.

Marrakchi, F., Ahmed, M. J., Khanday, W. A., Asif, M., Hameed, B. H. 2017. Mesoporous-activated carbon prepared from chitosan flakes via single-step hydroxide activation for the adsorption of methylene blue. *Int. J. Biol. Macromol.,* 98, 233-239.

Mashkoor, F., Nasar, A. 2019. Preparation, characterization and adsorption studies of the chemically modified *luffa aegyptica* peel as a potential adsorbent for the removal of malachite green from aqueous solution. *J. Mol. Liq.,* 274, 315-327.

Moreno-Marenco, A. R., Giraldo, L., Moreno-Piraján, J. C. 2020. Adsorption of n-butylparaben from aqueous solution on surface of modified granular activated carbons prepared from African palm shell: thermodynamic study of interactions. *J. Environ. Chem. Eng.,* 103969.

Mota, H. P., Quadrado, R. F. N., Burgo, T. A. L., Iglesias, B. A., Fajardo, A. R. 2020. Polysaccharide/Fe(III)-porphyrin hybrid film as catalyst for oxidative decolorization of toxic azo dyes: An approach for wastewater treatment. *Arab. J. Chem.,* 13, 7, 5923-5938.

Noor, N. M., Shariff, A., Abdullah, N., Aziz, N. S. M. 2019. Temperature effect on biochar properties from slow pyrolysis of coconut flesh waste. *Mal. J. Fund. Appl. Sci.,* 15, 153-158.

Pereira, L. A., Couto, A. B., Almeida, D. A. L., Ferreira, N. G. 2020. Singular properties of boron-doped diamond/carbon fiber composite as anode in brilliant green dye electrochemical degradation. *Diam. Relat. Mater.,* 103, 107708.

Putniss, A. 1995. Introduction To Mineral Sciences. *Cambridge University Press, Melbourne.*

Rahim, A. R. A., Kuanaseaan, K., Shehzad, N., Rabat, N. E., Johari, K., Mat, H. 2019. Synthesis and characterization of coconut pith char adsorbents for carbon dioxide capture. *Mal. J. Fund. Appl. Sci.,* 15, 803-805.

Shakib, F., Dadvand Koohi, A., Kamran Pirzaman, A. 2017. Adsorption of methylene blue by using novel chitosan-g-itaconic acid/bentonite nanocomposite – equilibrium and kinetic study. *Water Sci. Technol.,* 75, 1932-1943.

Shamsuddin, M. S., Yusoff, N. R. N., Sulaiman, M. A. 2016. Synthesis and characterization of activated carbon produced from kenaf core fiber using H_3PO_4 activation. *Procedia Chem.,* 19, 558-565.

Sharma, G., Sharma, S., Kumar, A., Naushad, M., Du, B., Ahamad, T., Ghfar, A. A., Alqadami, A. A. J., Stadler, F. 2019. Honeycomb structured activated carbon synthesized from pinus roxburghii cone as effective bioadsorbent for toxic malachite green dye. *J. Water Process Eng.,* 32, 100931.

Sips, R. 1948. Combined form of Langmuir and Freundlich equations. *J. Chem. Phys.,* 16, 490-495.

Temkin, M. I., Pyzhev, V. 1940. Kinetics of ammonia synthesis on promoted iron catalyst. *Acta Physiochimica U.S.S.R.,* 12, 327-356.

Thanarasu, A., Periyasamy, K., Manickam Periyaraman, P., Devaraj, T., Velayutham, K., Subramanian, S. 2020. Comparative studies on adsorption of dye and heavy metal ions from effluents using eco-friendly adsorbent. *Mater. Today.* In press.

Tunc, O., Tanac, H., Aksu, Z. 2009. Potential use of cotton plant wastes for the removal of remazol black B reactive dye. *J. Hazard. Mater.,* 163, 187-198.

Vega-Negron, A. L., Alamo-Nole, L., Perales-Perez, O., Gonzalez-Mederos, A. M., Jusino-Olivencia, C., Roman-Velazquez, F. R. 2018. Simultaneous adsorption of cationic and anionic dyes by chitosan/cellulose beads for wastewaters treatment. *Int. J. Environ. Res.,* 12, 59-65.

Vieth, W. R., Sladek, K. J. 1965. A model for diffusion in glassy polymer. *Journal Of Colloid Science,* 20, 1014-1033.

Weber, W. J., Morris, J. C. 1962. Kinetics of adsorption on carbon from solution. *J. Sanit. Eng. Div.,* 89, 31-59.

Weng, C. H., Lin, Y. T., Tzeng, T. W. 2009. Removal of methylene blue from aqueous solution by adsorption onto pineapple leaf powder. *J. Hazard. Mater.,* 170, 417-424.

Zhi, L. L., Zaini, M. A. A. 2019. Rhodamine B dyes adsorption on palm kernel shell based activated carbons. *Mal. J. Fund. Appl. Sci.,* 15, 743-747.

Zhou, L., Yu, Q., Cui, Y., Xie, F., Li, W., Li, Y., Chen, M. 2017. Adsorption properties of activated carbon from reed with a high adsorption capacity. *Ecol. Eng.,* 102, 443-450.

Zhou, X., Zhang, J., Pan, Z., Li, D. 2019. Review of methods for the detection and determination of malachite green and leuco-malachite green in aquaculture. *Crit. Rev. Anal. Chem.,* 49, 1-20.

Zhu, M., Yin, X., Chen, W., Yi, Z., Tian, H. 2018. Removal of sulphate from mine waters by electrocoagulation/rice straw activated carbon adsorption coupling in a batch system: optimization of process via response surface methodology. *J. Water Reuse Desal.,* 9, 163-172.

Zhu, Y., Wang, W., Ni, J., Hu, B. 2020. Cultivation of granules containing anaerobic decolorization and aerobic degradation cultures for the complete mineralization of azo dyes in wastewater. *Chemosphere,* 246, 125753.